TGF-β Signalling Drives Chemotaxis of Human Induced Pluripotent Stem Cell-Derived Cardiomyocytes in Response to MI Stimulus

Laura Deelen, Kazuya Kobayashi, Alia Hafiz Abbas Gasim, Fiona Lewis-McDougall*, Ken Suzuki*

Centre for Microvascular Research, William Harvey Research Institute, Faculty of Medicine and Dentistry, Queen Mary University of London, UK

*Joint corresponding authors: f.lewis@qmul.ac.uk, ken.suzuki@qmul.ac.uk

This study was funded by the British Heart Foundation (MRes/PhD DTP Programme, FS/19/62/34901).

ABSTRACT

Human induced pluripotent stem cell-derived cardiomyocytes (hiPSC-CMs) hold significant promise for cardiac regeneration therapies. However, the efficacy of such treatments depends on the ability of transplanted cells to migrate and integrate into the damaged myocardium, a process that remains poorly understood. In this study, we investigated the migratory behaviour of hiPSC-CMs using homogenised rat MI tissue to simulate myocardial infarction (MI) *in vitro*. Transwell migration assays demonstrated a concentration-dependent chemotactic response, with hiPSC-CM migration increasing up to threefold toward MI tissue homogenate. Wound healing assays further confirmed enhanced migration under MI-mimetic conditions. Bulk RNA sequencing revealed activation of the TGF-β signalling pathway as a key regulator of this response. Inhibition of TGF-β signalling, both pharmacologically and through antibody neutralisation, significantly reduced hiPSC-CM migration. These findings uncover a previously underappreciated chemotactic capability of hiPSC-CMs and identify TGF-β signalling as a central mediator, offering new mechanistic insights and potential therapeutic targets to improve the integration and efficacy of hiPSC-CM-based cardiac regeneration strategies.

INTRODUCTION

Myocardial infarction (MI) is one of the most common causes of ischaemic heart failure (HF), for which the prognosis is only 50% within 5 years of diagnosis[1]. During MI, persistent coronary artery obstruction leads to the irreversible loss of billions of cardiac cells including cardiomyocytes (CMs). Currently the only established treatment for end-stage HF patients is heart transplantation or the permanent implantation of a left ventricular assist device as an emerging alternative[2,3]. However, these approaches have several limitations, including high costs, complications related to immunosuppression or anticoagulants, and psychological strain for patients. Myocardial regeneration therapy has drawn major attention over the last few decades as an innovative treatment to restore functional CMs after MI and improve prognosis through enhanced cardiac function. Human induced pluripotent stem cells (hiPSCs) have gained popularity as donor cells for myocardial regeneration therapy due to their unlimited self-renewal, autologous clinical potential and robust cardiomyogenic differentiation potency. Therefore, the transplantation of hiPSC-derived CMs (hiPSC-CMs) has become an active field of research for the treatment of post-MI HF.

Promising methods for delivery of replacement CMs to the heart include epicardial placement and intramyocardial injection of cell suspension or spheroids[4–6]. The migration of hiPSC-CMs following transplantation is a critical determinant of the success of cell-based cardiac regenerative therapies. Following epicardial delivery, a significant proportion of hiPSC-CMs have been shown to remain localized on the heart surface, failing to penetrate and integrate with the host myocardium [7,8]. While intramyocardial injection offers more precise delivery into damaged myocardial regions, even this method relies on the transplanted cells' ability to migrate within the myocardium to establish functional integration with surviving host cardiomyocytes. Such migration is essential for structural continuity, electrical coupling, and

51 functional contribution to the regenerating heart. Therefore, limited intramyocardial migration
52 remains a major barrier to the success of cell-based therapies.

53 Previous studies have begun to shed light on the migratory capacity of human stem cell-derived
54 cardiomyocytes. Moyes et al. demonstrated that human embryonic stem cell-derived
55 cardiomyocytes (hESC-CMs) exhibit enhanced migration *in vitro* in response to Wnt5a and
56 fibronectin[9]. Another study identified BANCR, a primate-specific long non-coding RNA, as a
57 positive regulator of hiPSC-CM migration[10]. Additional research on embryonic and neonatal
58 CM migration has revealed that non-coding RNAs and developmentally regulated proteins may
59 influence CM motility[11–14].

60 Among the key pathways implicated in cardiomyocyte migration during regeneration is the
61 TGF-β signalling pathway. In zebrafish, which possess innate cardiac regenerative capacity,
62 SMAD3-dependent TGF-β signalling is essential for CM migration into damaged tissue and
63 chemical inhibition of TGF-β signalling significantly impairs this migratory response[15].
64 Moreover, suppression of TGF-β–Smad3 signalling has been shown to inhibit an EMT-like
65 response in CMs during zebrafish heart regeneration following ventricular ablation[16].

66 It is known that MI triggers the release of numerous signalling molecules into the surrounding
67 tissue, some of which may serve as chemoattractants for migratory cells. While adult CMs
68 likely lack the capacity to respond to these cues, hiPSC-CMs due to their fetal-like phenotype,
69 may retain an intrinsic ability to migrate in response to such signals, similar to regenerative
70 responses observed in zebrafish[17].

71 In this study, we aimed to investigate the migratory behaviour of hiPSC-CMs in response to
72 infarct-associated signals. To this end, we employed transwell migration and wound healing
73 assays to assess hiPSC-CM migration *in vitro*, using rat myocardial infarction MI tissue
74 homogenate to mimic the post-MI microenvironment. Furthermore, we conducted bulk RNA

sequencing on migrated and non-migrated hiPSC-CMs to identify key molecular pathways involved in this response.

Together, this study provides novel mechanistic insights into the chemotactic and migratory behaviour of hiPSC-CMs in the context of MI. These findings provide new insights into the migratory behaviour of hiPSC-CMs in response to infarct-associated cues and highlight molecular targets, such as TGF-β signalling, that could be modulated to enhance cell integration and improve functional outcomes in post-MI cardiac regenerative therapies.

RESULTS

HiPSC-CMs exhibit a concentration-dependent chemotactic response to rat MI tissue homogenate

Four hiPSC lines (hiPSC-A, B, C and D) were used in this study, each were confirmed to express surface and intracellular pluripotency markers and were karyotypically normal (Fig. S1). To generate hiPSC-CMs, we utilised the well-established protocol published by Burridge et. al[18] or a commercial CM Differentiation Kit (STEMCELL Technologies) as an alternative. Spontaneous cell contractions were observed between days 7 and 11 post- induction of differentiation (Vid. S1).

Cardiomyocyte identity and differentiation efficiency were validated using flow cytometry, RT-PCR, and immunofluorescence staining. The Burridge protocol consistently yielded cTnT-positive cells across all four hiPSC lines (Fig. S2A), with protein expression of cTnT, NKX2.5, and α-actinin confirmed at day 15 (Fig. S2B). Gene expression profiling showed downregulation of pluripotency markers (POU5F1, NANOG, SOX2), transient upregulation of early mesoderm markers (MESP1, KIT), and increased expression of cardiomyocyte markers (NKX2-5, TNNT2, MYL7, MYL2) over time (Fig. S2C–G). For all downstream

experiments, only differentiations achieving >60% cTnT+ cells by flow cytometry were included.

To assess whether MI tissue exerts a chemotactic effect on hiPSC-CMs, we developed a transwell migration (TWM) assay (Fig. 1A). Human iPSC-CM-A cells were seeded in the upper chamber and exposed to various dilutions of MI homogenate, derived from rat left ventricular tissue harvested 1-day post-MI. After 24 hours, migrated cells on the lower membrane surface were stained with DAPI and quantified (Fig. 1B–D). A significant, concentration-dependent increase in hiPSC-CM-A migration was observed in response to MI homogenate compared to control medium, with a peak 3-fold increase at a 1:10 dilution (Fig. 1C). Similarly, hiPSC-CM-B showed a robust 3-fold increase at the same dilution (Fig. 1D), and comparable results were seen in hiPSC-CM-C (Fig. S3).

We next explored whether the duration of hiPSC-CM culture influences their migratory capacity, given the known association between cardiomyocyte maturation and reduced motility[19,20]. Cells were assessed at various differentiation time points (day 15 to day 45) in the TWM assay. For hiPSC-CM-A, migration remained stable (~20–30%) across this time frame, with no statistically significant changes (Fig. 1E). In contrast, hiPSC-CM-B displayed a time-dependent decline in migration, decreasing from 28% at day 15 to just 9% by day 45 (Fig. 1F). These findings suggest cell line-specific differences in how prolonged culture impacts migratory ability.

Our transwell migration assays demonstrate that rat MI tissue homogenate induces a strong, concentration-dependent chemotactic response in hiPSC-CMs across multiple cell lines. Furthermore, cell line-specific and temporal factors influence the persistence of this migratory capacity during extended in vitro culture. These findings underscore the importance of

122 accounting for both biological variability and maturation state when considering hiPSC-CMs
123 for regenerative applications.

124 ***An MI Stimulus Accelerates Collective hiPSC-CM Migration***

125 To further investigate the impact of MI-associated cues on hiPSC-CM migration, we employed
126 a wound healing assay to assess collective migration and wound closure dynamics. Human
127 iPSC-CM-D monolayers were incubated with LV tissue homogenate from either MI or non-MI
128 (sham) rats, and wound closure was assessed 4 hours after scratch injury (Fig. 2A–C).

129 Exposure to MI homogenate (1:10 dilution) significantly enhanced wound closure compared
130 to control medium (16.6 ± 6.9% vs. 8.5 ± 5.2%, respectively). This was accompanied by a
131 substantial increase in the cell front migration speed, which more than doubled from 6.2 ± 3.7
132 μm/h in control conditions to 14.3 ± 4.4 μm/h in the presence of MI homogenate. Our observed
133 migration speeds closely match those reported for hESC-CMs [9], reinforcing the biological
134 validity of the model.

135 Interestingly, exposure to non-MI (sham) LV homogenate also resulted in enhanced wound
136 closure (14.7 ± 4.6%) and increased migration speed (11.2 ± 4.0 μm/h) (Fig. 2A-C), though
137 both metrics remained lower than those observed with MI homogenate. To further explore this
138 observation, we conducted a transwell migration assay. Consistent with the wound healing
139 results, non-MI homogenate induced a significant increase in hiPSC-CM migration relative to
140 medium alone, but to a lesser extent than MI homogenate (Fig. 2D). This suggests that while
141 sham homogenate does have chemokinetic effects, likely due to intracellular content release
142 during tissue homogenisation, it lacks the full complement of injury-associated chemotactic
143 cues present in the MI tissue.

144

145 ***Migrated hiPSC-CMs exhibit a differential gene expression profile from non-migrated***
146 ***hiPSC-CMs***

147 To identify pathways involved in hiPSC-CM migration, we employed a TWM assay in which
148 day 15 hiPSC-CMs were exposed to rat MI homogenate for 24 hours. Migrated cells were
149 collected from the lower surface of the membrane, while non-migrated cells were harvested
150 from the upper surface. RNA was extracted from both populations for bulk RNA sequencing
151 to comprehensively profile gene expression differences.

152 Principal component analysis (PCA) revealed clear segregation between the two hiPSC lines
153 (hiPSC-CM-A and hiPSC-CM-B) along PC1, and between migrated and non-migrated samples
154 of each line along PC2 (Fig. 3A). Together, PC1 and PC2 accounted for 91.53% of the total
155 variance, indicating these components capture the main sources of gene expression variability.
156 Notably, gene expression changes were more pronounced in hiPSC-CM-A than hiPSC-CM-B,
157 highlighting inter-line variability.

158 To confirm cardiomyocyte identity, expression of canonical CM markers (TNNT2, NKX2-5,
159 MYL7) was examined, showing comparable levels between migrated and non-migrated groups
160 in both cell lines (Table S1). CM subtype markers indicated a heterogeneous population
161 consisting of atrial (NR2F2), ventricular (MYL2, IRX4), and nodal (TBX18, HCN4) subtypes,
162 consistent with expectations from the Burridge differentiation protocol (Fig. S2, Table S1). The
163 immature phenotype of hiPSC-CMs was reflected by higher expression of fetal isoforms
164 TNNI1 and MYH6 relative to adult isoforms TNNI3 and MYH7. Evaluation of potential
165 contaminating cell types revealed low expression of cardiac fibroblast markers DDR2 and
166 CD90 (THY1), and absence of endothelial marker CD31 in both lines (Table S1).

167

168 Following 24-hour incubation with MI homogenate, differential gene expression analysis
169 identified 849 genes significantly altered in migrated versus non-migrated hiPSC-CM-A cells
170 (598 upregulated and 248 downregulated; adjusted p-value < 0.05, log2 fold change > 1) (Fig.
171 3B). In contrast, only 46 genes were significantly differentially expressed in hiPSC-CM-B (38
172 upregulated, 8 downregulated). Integrating data from both lines yielded a consensus panel of
173 28 differentially expressed genes (DEGs) (Fig. 3C–D). Interestingly, proliferative markers
174 MKI67 and CDK1 were present in this panel, suggesting that migrated hiPSC-CMs in both
175 lines were more proliferative then non-migrating hiPSC-CMs.

176

177 From this panel, 14 genes of interest were selected for validation by RT-qPCR across hiPSC-
178 CM-A, -B, and -C lines, confirming reproducible upregulation (Fig. S4). Gene Ontology (GO)
179 enrichment analysis revealed that DEGs were predominantly associated with extracellular
180 matrix organization, cell migration, and chemotaxis (Table S2). Ingenuity Pathway Analysis
181 (IPA, QIAGEN) further identified cellular movement as a top molecular and cellular function
182 linked to the differentially expressed genes in both datasets (Fig. 3F), supporting the ability of
183 our model to uncover key regulators of hiPSC-CM migration

184

185 ***Inhibition of TGF-β signalling reduces MI homogenate-induced hiPSC-CM migration***

186 To investigate potential upstream regulators driving hiPSC-CM migration, we examined links
187 between DEGs identified in our RNA-seq datasets. Among the 28 DEGs shared between
188 migrated hiPSC-CM-A and hiPSC-CM-B, seven genes (SOX17, BMP6, TGFBI, SPP1, NT5E,
189 HMGA2, and DACT2) have previously been directly associated with TGF-β signalling
190 pathways [23–28]. Furthermore, Ingenuity Pathway Analysis (IPA) identified TGF-β1 as a central

upstream regulator associated with 12 of the 28 DEGs, implicating it in the observed migratory behaviour.

TGF-β signalling is known to be upregulated in the myocardium following MI [29,30] and plays a crucial role in heart regeneration in the zebrafish model, particularly by inducing an epithelial-to-mesenchymal transition (EMT)-like response in cardiomyocytes, which promotes migratory activity [15, 16]. Notably, HMGA2, one of the DEGs identified in our study, is a well-characterized mediator of TGF-β-induced EMT [28].

To assess the functional relevance of TGF-β signalling in hiPSC-CM migration, we used the pharmacological inhibitor SB431542, which selectively blocks the kinase activity of the TGF-β type I receptor (ALK5) [31]. In a scratch wound assay, treatment with SB431542 from 1 hour to 20 hours post-incubation with MI homogenate significantly reduced wound closure compared to MI homogenate alone (Fig. 4A). Similarly, cell front migration velocity was markedly decreased in the presence of SB431542, returning to baseline levels observed in control medium (Fig. 4B). Notably, the most pronounced effect occurred during the first 8 hours of incubation, suggesting that TGF-β signalling plays an early and critical role in initiating hiPSC-CM migration.

We then confirmed the presence of TGF-β1 protein in the MI homogenate, measuring 1,014 ± 183 ng/mL, which was significantly higher than in non-MI (sham) homogenate (540 ± 146 ng/mL, Fig. S5). The detectable level of TGF-β1 in sham homogenate may account for its observed partial chemokinetic and chemotactic effects on hiPSC-CM migration (as described in Fig. 2).

To further confirm the involvement of TGF-β signalling, we performed a transwell migration assay. After 4 hours of incubation, the addition of 10 μM SB431542 to MI homogenate

215 significantly reduced the number of migrated hiPSC-CMs (Fig. 4C–D). Similarly, the
216 application of a neutralising anti–TGF-β1 antibody attenuated MI homogenate-induced
217 migration. In hiPSC-CM-A, neutralisation led to a significant reduction in migrated cells (Fig.
218 4E), while hiPSC-CM-B showed a strong decreasing trend ($p = 0.05$, Fig. 4F).

219 These findings provide robust evidence that TGF-β1 is a key mediator of the migratory
220 response of hiPSC-CMs to MI tissue stimuli. Pharmacological inhibition and antibody-based
221 neutralisation both significantly impaired migration, supporting a causal role for TGF-β
222 signalling in promoting hiPSC-CM motility. These results highlight TGF-β1 as a potential
223 therapeutic target to modulate transplanted cell behaviour in cardiac regeneration strategies.

224 **DISCUSSION**

225 This study provides, to our knowledge, the first comprehensive characterisation of the
226 migratory capacity of hiPSC-CMs in response to factors derived from infarcted myocardium.
227 Using two gold-standard *in vitro* migration models, transwell migration (TWM) and scratch
228 wound assays, we demonstrated that hiPSC-CMs exhibit significant, concentration-dependent
229 migratory responses when exposed to rat MI tissue homogenate. By employing multiple hiPSC
230 lines, we confirmed the biological reproducibility of this migratory behaviour, establishing it
231 as a previously unknown but relevant property of hiPSC-CMs in the context of MI.

232 The TWM model enabled the physical separation of migrated and non-migrated hiPSC-CM
233 populations, allowing for bulk RNA sequencing to uncover gene expression differences
234 potentially underpinning migration. Among the 28 DEGs common to two hiPSC lines, multiple
235 were linked to the TGF-β signalling pathway, which was further validated through
236 pharmacological and antibody-based inhibition. TGF-β has long been proposed as a
237 chemoattractant [32,33] and is known to regulate migration in diverse cell types [34–36] . Within the
238 heart, it has been shown to influence cell migration during development and post-injury repair
239 [37] . In regenerative models such as zebrafish, TGF-β signalling plays a critical role in cardiac
240 regeneration following injury, mediating cardiomyocyte migration through an EMT-like
241 process [15,16]. Our findings are consistent with these models and extend them by demonstrating
242 that TGF-β1 also promotes hiPSC-CM migration in response to an MI stimulus.

243 We confirmed that MI homogenate contains significantly higher levels of TGF-β1 than non-
244 MI (sham) homogenate and demonstrated that inhibiting TGF-β signalling with SB431542 or
245 a TGF-β neutralising antibody significantly impaired hiPSC-CM migration. These results
246 provide functional evidence that TGF-β1 is an active component of the infarcted myocardial
247 microenvironment driving hiPSC-CM motility, and position it as a candidate target to enhance
248 integration of transplanted cells into injured myocardium. However, the context-dependent

249 nature of TGF-β signalling, which can elicit both beneficial and deleterious effects depending
250 on cell type and injury phase, must be carefully considered [38-41].

251 Interestingly, our transcriptomic analysis also identified a proliferative gene expression profile
252 in migrated hiPSC-CMs, including upregulation of MKI67 and CDK1. This suggests that
253 migrated cells may possess enhanced proliferative potential, which could represent an added
254 advantage following transplantation, contributing not only to cell engraftment but also to
255 remuscularisation of infarcted tissue. Further studies are warranted to characterise and
256 potentially harness this proliferative capacity *in vivo*.

257 We also examined the relationship between hiPSC-CM maturation and migration potential. As
258 expected, prolonged culture led to either stable or reduced migratory capacity, depending on
259 the cell line. While hiPSC-CM-A maintained consistent migration rates up to day 45 of
260 differentiation, hiPSC-CM-B showed a marked decline over time. This suggests that cell line-
261 intrinsic properties, alongside maturation status, influence migratory ability. Determining the
262 optimal differentiation stage for transplantation will be critical, particularly as hiPSC-CMs
263 undergo changes in metabolism, electrophysiology, and stress responses with maturation, all
264 of which could impact therapeutic efficacy.

265 Our findings also raise important questions regarding cardiomyocyte subtype-specific
266 migration. We observed early expression of the atrial marker MLC2a, which declined over
267 time, while ventricular marker MLC2v increased, typical of CM maturation. However, there
268 were no significant differences in the expression of MYL2 or MYL7 between migrated and
269 non-migrated cells, suggesting that both atrial- and ventricular-like hiPSC-CMs (and double-
270 positive cells) can respond to migratory cues. Nevertheless, recent protocols enabling the
271 generation of highly enriched ventricular hiPSC-CMs [42] offer the opportunity to more precisely
272 investigate the influence of CM subtype on migratory behaviour in future studies.

In summary, this study reveals novel insights into the migratory potential of hiPSC-CMs, identifies TGF-β1 as a key mediator of this response, and highlights the importance of cell-intrinsic properties, maturation state, and myocardial context in modulating migration. These findings contribute to our understanding of how transplanted hiPSC-CMs might interact with the post-MI environment, with potential implications for improving cell therapy strategies aimed at cardiac regeneration. Targeting the migratory behaviour of hiPSC-CMs will enable us to promote effective cell engraftment and integration, ultimately supporting functional repair of the injured heart.

Bibliography

1. Tsao, C. W. *et al.* Heart Disease and Stroke Statistics—2023 Update: A Report From the American Heart Association. *Circulation* **147**, E93–E621 (2023).

2. Kormos, R. L. *et al.* The Society of Thoracic Surgeons Intermacs Database Annual Report: Evolving Indications, Outcomes, and Scientific Partnerships. *Ann Thorac Surg* **107**, 341–353 (2019).

3. Slaughter, M. S. *et al.* Advanced heart failure treated with continuous-flow left ventricular assist device. *New England Journal of Medicine* **361**, 2241–2251 (2009).

4. Kawamura, T. *et al.* Safety confirmation of induced pluripotent stem cell-derived cardiomyocyte patch transplantation for ischemic cardiomyopathy: first three case reports. *Front Cardiovasc Med* **10**, 1–9 (2023).

5. Shiba, Y. *et al.* Allogeneic transplantation of iPS cell-derived cardiomyocytes regenerates primate hearts. *Nature* **538**, 388–391 (2016).

6. Safety and Efficacy of Induced Pluripotent Stem Cell-derived Engineered Human Myocardium as Biological Ventricular Assist Tissue in Terminal Heart Failure. ClinicalTrials.gov identifier: NCT04396899. Updated March 27, 2023. Accessed February 06,2025. https://clinicaltrials.gov/study/NCT04396899

7. Miki, K. *et al.* Bioengineered Myocardium Derived from Induced Pluripotent Stem Cells Improves Cardiac Function and Attenuates Cardiac Remodeling Following Chronic Myocardial Infarction in Rats. *Stem Cells Transl Med* **1**, 430–437 (2012).

8. Hata, H. *et al.* Engineering a novel three-dimensional contractile myocardial patch with cell sheets and decellularised matrix. *European Journal of Cardio-thoracic Surgery* **38**, 450–455 (2010).

9. Moyes, K. W. *et al.* Human Embryonic Stem Cell-Derived Cardiomyocytes Migrate in Response to Gradients of Fibronectin and Wnt5a. *Stem Cells Dev* **22**, 2315–2325 (2013).

10. Wilson, K. D. *et al.* Endogenous Retrovirus-Derived lncRNA BANCR Promotes Cardiomyocyte Migration in Humans and Non-human Primates. *Dev Cell* **54**, 694-709.e9 (2020).

11. Hosen, M. R. *et al.* Airn Regulates Igf2bp2 Translation in Cardiomyocytes. *Circ Res* **122**, 1347–1353 (2018).

12. Qin, X., Gao, S., Yang, Y., Wu, L. & Wang, L. microRNA-25 promotes cardiomyocytes proliferation and migration via targeting Bim. *J Cell Physiol* **234**, 22103–22115 (2019).

13. Bergeron, A. *et al.* Filamentous nestin and nonmuscle myosin IIB are associated with a migratory phenotype in neonatal rat cardiomyocytes. *J Cell Physiol* **236**, 1281–1294 (2021).

14. Bock-Marquette, I., Saxena, A., White, M. D., DiMaio, J. M. & Srivastava, D. Thymosin β4 activates integrin-linked kinase and promotes cardiac cell migration, survival and cardiac repair. *Nature* **432**, 466–472 (2004).

15. Chablais, F. & Jaźwińska, A. The regenerative capacity of the zebrafish heart is dependent on TGFβ signaling. *Development* **139**, 1921–1930 (2012).

16. Peng, Y. *et al.* Inhibition of TGF-β/Smad3 Signaling Disrupts Cardiomyocyte Cell Cycle Progression and Epithelial–Mesenchymal Transition-Like Response During Ventricle Regeneration. *Front Cell Dev Biol* **9**, 1–14 (2021).

17. Itou, J. *et al.* Migration of cardiomyocytes is essential for heart regeneration in zebrafish. *Development (Cambridge)* **139**, 4133–4142 (2012).

18. Burridge, P. W., Holmström, A. & Wu, J. C. Chemically Defined Culture and Cardiomyocyte Differentiation of Human Pluripotent Stem Cells. *Curr Protoc Hum Genet* **87**, 21.3.1-21.3.15 (2015).

19. Burridge, P. W. *et al.* Chemically defined generation of human cardiomyocytes. *Nat Methods* **11**, 855–860 (2014).

20. Lundy, S. D., Zhu, W. Z., Regnier, M. & Laflamme, M. A. Structural and functional maturation of cardiomyocytes derived from human pluripotent stem cells. *Stem Cells Dev* **22**, 1991–2002 (2013).

21. Zuppinger, C. *et al.* Characterization of cytoskeleton features and maturation status of cultured human iPSC-derived cardiomyocytes. *European Journal of Histochemistry* **61**, 145–153 (2017).

22. Ormrod, B. & Ehler, E. Induced pluripotent stem cell-derived cardiomyocytes—more show than substance? *Biophys Rev* **15**, 1941–1950 (2023).

23. Cappelli, C. *et al.* The TGF-β profibrotic cascade targets ecto-5′-nucleotidase gene in proximal tubule epithelial cells and is a traceable marker of progressive diabetic kidney disease. *Biochim Biophys Acta Mol Basis Dis* **1866**, 165796 (2020).

24. Dituri, F., Cossu, C., Mancarella, S. & Giannelli, G. The Interactivity between TGFβ and BMP Signaling in Organogenesis, Fibrosis, and Cancer Activated Protein Kinases (MAPKs, namely Extracellular Receptor Kinase 1 and 2-ERK1/2. *Cells* **8**, 1–21 (2019).

25. Hou, J. *et al.* DACT2 regulates structural and electrical atrial remodeling in atrial fibrillation. *J Thorac Dis* **12**, 2039–2048 (2020).

26. Kramerova, I. *et al.* Spp1 (osteopontin) promotes TGFβ processing in fibroblasts of dystrophin-deficient muscles through matrix metalloproteinases. *Hum Mol Genet* **28**, 3431 (2019).

27. Lange, A. W., Keiser, A. R., Wells, J. M., Zorn, A. M. & Whitsett, J. A. Sox17 promotes cell cycle progression and inhibits TGF-β/Smad3 signaling to initiate progenitor cell behavior in the respiratory epithelium. *PLoS One* **4**, (2009).

28. Thuault, S. *et al.* Transforming growth factor-β employs HMGA2 to elicit epithelial-mesenchymal transition. *Journal of Cell Biology* **174**, 175–183 (2006).

29. Li, Q., Xu, Y., Li, X., Guo, Y. & Liu, G. Inhibition of Rho-kinase ameliorates myocardial remodeling and fibrosis in pressure overload and myocardial infarction: Role of TGF-β1-TAK1. *Toxicol Lett* **211**, 91–97 (2012).

30. Vilahur, G. *et al.* Molecular and cellular mechanisms involved in cardiac remodeling after acute myocardial infarction. *J Mol Cell Cardiol* **50**, 522–533 (2011).

31. Inman, G. J. *et al.* SB-431542 is a potent and specific inhibitor of transforming growth factor-β superfamily type I activin receptor-like kinase (ALK) receptors ALK4, ALK5, and ALK7. *Mol Pharmacol* **62**, 65–74 (2002).

32. Reibman, J. *et al.* Transforming growth factor β1, a potent chemoattractant for human neutrophils, bypasses classic signal-transduction pathways. *Proc Natl Acad Sci U S A* **88**, 6805–6809 (1991).

33. Wahl, S. M. *et al.* Transforming growth factor type β induces monocyte chemotaxis and growth factor production. *Proc Natl Acad Sci U S A* **84**, 5788–5792 (1987).

34. Liu, Z., Yi, L., Du, M., Gong, G. & Zhu, Y. Overexpression of TGF-β enhances the migration and invasive ability of ectopic endometrial cells via ERK/MAPK signaling pathway. *Exp Ther Med* 4457–4464 (2019) doi:10.3892/etm.2019.7522.

35. Melzer, C., von der Ohe, J., Hass, R. & Ungefroren, H. TGF-β-dependent growth arrest and cell migration in benign and malignant breast epithelial cells are antagonistically controlled by Rac1 and Rac1b. *Int J Mol Sci* **18**, (2017).

36. Zhao, W. *et al.* Effect of TGF-β1 on the Migration and Recruitment of Mesenchymal Stem Cells after Vascular Balloon Injury: Involvement of Matrix Metalloproteinase-14. *Sci Rep* **6**, 1–11 (2016).

37. Azhar, M. *et al.* Transforming growth factor beta in cardiovascular development and function. *Cytokine Growth Factor Rev* **14**, 391–407 (2003).

38. Hanna, A. & Frangogiannis, N. G. The Role of the TGF-β Superfamily in Myocardial Infarction. *Front Cardiovasc Med* **6**, 1–15 (2019).

39. Dobaczewski, M., Gonzalez-Quesada, C. & Frangogiannis, N. G. The extracellular matrix as a modulator of the inflammatory and reparative response following myocardial infarction. *Journal of Molecular and Cellular Cardiology* Preprint at https://doi.org/10.1016/j.yjmcc.2009.07.015 (2010).

40. Yi, X. *et al.* Hepatocyte growth factor regulates the TGF-β1-induced proliferation, differentiation and secretory function of cardiac fibroblasts. *Int J Mol Med* **34**, 381–390 (2014).

41. Pardali, E. & Dijke, P. Transforming growth factor-beta signalling and tumor angiogenesis. *Mol Cell* **14**, 4848–4861 (2009).

42. Dark, N. *et al.* Generation of left ventricle-like cardiomyocytes with improved structural, functional, and metabolic maturity from human pluripotent stem cells. *Cell Reports Methods* **3**, 100456 (2023).

393 **METHODS AND MATERIALS**

394 ***Human iPSC culture***

395 Four hiPSC lines were obtained from the European Bank for Induced Pluripotent Stem Cells
396 (EBiSC) and maintained in feeder-free, serum-free 2D culture at 37°C and 5% CO_2. For CM
397 differentiation, hiPSCs were grown in E8 Flex medium (Thermofisher) on recombinant human
398 vitronectin (rhVTN)-coated plates for 3-4 days until reaching approximately ~85% confluency.
399 Differentiation into cardiomyocytes was initiated using a protocol adapted from Burridge et
400 al.[18] Briefly, hiPSCs were incubated in CDM3 medium; RPMI 1640 supplemented with 75
401 mg/mL recombinant human albumin (Merck) and 64 mg/mL L-ascorbic acid 2-phosphate
402 (Merck) with the addition of 6 μM CHIR99021 (Cambridge Bioscience) for 48 hours. On day
403 2, the medium was replaced with CDM3 containing 2 μM Wnt-C59, and from day 4 onwards
404 cells were maintained in CDM3 alone, with media refreshed every two days. Alternatively,
405 where indicated, hiPSC-CMs were generated using a commercially available Cardiomyocyte
406 Differentiation Kit (STEMCELL Technologies), following the manufacturer's instructions.

407

408 ***Heart tissue homogenisation***

409 Adult male Sprague-Dawley rats underwent either MI induction via left coronary artery (LCA)
410 ligation or a sham surgical procedure. For MI, the LCA was ligated at the level of the lower
411 edge of the left atrial appendage via left thoracotomy under isoflurane anaesthesia and
412 mechanical ventilation. Successful induction of ischaemia was confirmed by regional
413 epicardial colour change and the presence of dyskinesia. Following chest and skin closure,
414 animals were extubated and allowed to recover in their cage. Sham-operated animals
415 underwent an open-chest procedure without LCA ligation. All animals were sacrificed 24 hours

post-surgery. The left ventricular (LV) wall was then harvested, either freshly homogenised or snap-frozen in liquid nitrogen and stored at –80 °C for later use.

Tissue homogenisation was performed PBS supplemented with protease inhibitors (cOmplete™, EDTA-free Protease Inhibitor Cocktail; Sigma-Aldrich) using a Precellys 24 tissue homogeniser. Homogenates were centrifuged at 6,000 × g for 15 minutes, and the supernatant was collected for immediate use or stored at –80 °C for subsequent experiments.

All animal procedures were approved by the institutional ethics committee at Queen Mary University of London and the UK Home Office. Experiments conformed to the *Principles of Laboratory Animal Care* (National Society for Medical Research) and the *Guide for the Care and Use of Laboratory Animals* (U.S. National Institutes of Health, 1996).

Wound healing assay

Human iPSC-CMs were seeded at a density of ≥ 2.5 x 10^5 cells/cm^2 to form a confluent monolayer. To promote cell attachment, hiPSC-CMs were incubated overnight with 10 µM Y-27632 (Rock inhibitor; Cambridge BioScience). The following day, a scratch wound was generated across the hiPSC-CM monolayer using a sterile P1000 tip. After washing with PBS to remove detached cells, hiPSC-CMs were incubated for up to 24 hours with either cell media alone or medium supplemented with LV homogenate from MI or sham operated rat hearts (diluted as specified).

Cell migration was assessed by capturing images at defined time points using either a Keyence BZ-X810 microscope or an EVOS XL Core Cell Imaging System. Quantitative analysis was performed using ImageJ software. Percentage wound closure was calculated as follows;

$$\frac{wound\ area\ at\ 4h\ (\mu m^2) - initial\ wound\ area\ (\mu m^2)}{initial\ wound\ area\ (\mu m^2)}\ x\ 100$$

439

440 Cell front migration was calculated as follows;

441 $$\frac{wound\ area\ at\ 4h\ (\mu m^2) - initial\ wound\ area\ (\mu m^2)}{height\ of\ the\ image\ (\mu m)}$$

442 in which the height of the image represents the y-axis, to obtain the difference in horizontal
443 distance (x-axis), i.e., the cell front migration (µm). This number is then divided by the
444 incubation time to obtain the cell front migration speed (µm/h).

445

446 ***Transwell migration assay***

447 All TWM assays were performed in 24-well plates. Transwell inserts with 8 µM pore size
448 (Starstedt) were pre-coated on both sides with ~22 µg/cm^2 Geltrex Ready to Use
449 (Thermofisher) for 1h at 37°C. After aspiration of the residual coating, 1 x 10^5 hiPSC-CMs per
450 insert were seeded into the upper chamber in cardiomyocyte support medium supplemented
451 with 10 µM Y-27632 (Rock inhibitor)and incubated overnight to allow cell attachment. The
452 next day, the medium in the lower chamber was replaced with cell medium alone or medium
453 supplemented with LV homogenate from MI or sham operated rat hearts at the indicated
454 dilution. After 24 hours of incubation, cells were fixed in 4% paraformaldehyde for 15 mins at
455 room temperature (RT) followed by a PBS wash and incubation with DAPI for 15 mins at RT.
456 To ensure that only migrated cells on the lower surface were visualised, the upper surface of
457 the insert was gently swabbed with a cotton applicator to remove non-migrated cells. The
458 membranes were then carefully excised and mounted onto glass microscope slides. Images
459 were acquired on a Keyence BZ-X180 or Zeiss LSM800 microscope. Quantification of
460 migrated cells was performed using ImageJ software.

461

462 ***ELISA***

463 TGF-β1 levels were measured in homogentes from sham and MI tissues using a TGF-beta 1
464 Quantikine ELISA kit (R&D, Cat #DB100C). To activate latent TGF-β1, tissue supernatents
465 were incubated with 1M HCl for 10 mins, followed by neutralisation with 1.2M NaOH/0.5M
466 HEPES. Activated samples or standards were added to wells pre-coated with TGF-β1 capture
467 antibody, along with the assay diluent. After a 2h incubation at RT, plates werewashed four
468 times before addition of the TGF-β1 conjugate. Plates were then incubated for a further 2 hours,
469 followed by four washes. Substrate solution was then added and incubated for 30 mins at RT
470 in the dark. The reaction was stopped by the addition of Stop Solution and absorbance was
471 measured at with wavelength correction at 540 nm using a microplate reader.

472 ***Bulk RNAseq***

473 Human iPSCs were seeded onto transwell inserts at day 15 of CM differentiation, as previously
474 described. After 24 hours of incubation with a 1:10 dilution of left ventricular homogenate
475 from a MI rat heart in the lower compartment, culture media was aspirated and the inserts
476 washed in PBS. To isolate migrating and non-migrating cells, the upper and lower surfaces of
477 the inserts were swabbed separately.

478 .RNA was extracted by lysing the cells directly on the inserts using RLT lysis buffer from the
479 Qiagen RNeasy mini kit, following the manufacturer'sinstructions. Samples with RNA
480 integrity numbers (RIN)≥ 9.4 and a minimum input of 100ng of total RNA were used for bulk
481 RNAseq (20 million reads per samples). Library preparation and paired-end 150 bp sequencing
482 (PE150) were performed by Novogene Ltd, who also conducted downstream data analysis.

483

484 ***Immunocytochemistry***

485 Human iPSCs were harvested by incubation with EDTA for 3-5 mins, followed by gentle
486 detachment with culture media. Cells were seeded onto 16 mm coverslips in 12 well plates pre-
487 coated with rhVTN and cultured for 2-4 days before fixation with 4% paraformaldehyde in
488 PBS for 15 min at 37°C.

489 Ahead of immunostaining, hiPSC-CMs were replated overnight using the CM dissociation kit
490 (Thermofisher). Briefly, wells were washed twice with PBS before incubation with
491 CMdissociation medium at 37°C for 10-15 mins. Detached cells were collected usinga 10 mL
492 serological pipette and transferred into tubes containing CM support medium. After
493 centrifugation at 300 g for 5 min, the supernatant was removed, and the cell pellet was
494 resuspended in CM support medium supplemented with 5 µM Y-27632. Cells were seeded into
495 a new rhVTN-coated plate at the desired density ($\geq 2.5 \times 10^5$ cells/cm^2) and allowed to attach
496 overnight. The following day, cells were fixed with 4% paraformaldehyde in PBS for 15 mins
497 at 37°C.

498 After fixation, hiPSCs and hiPSC-CMs were washed and permeabilised with 0.1% Triton-X-
499 100 inPBS for 10 min at RT, then blocked using 10% donkey serum/PBS for 1h at RT. Primary
500 antibodies were applied overnight at 4°C in the dark. After washing, cells were incubated with
501 appropriate secondary antibodies for 30 mins at 37°C. DAPI was used as a nuclear counterstain.
502 All wash steps were performed with 0.1% Tween in PBS. Imaging was conducted using a Zeiss
503 LSM 800 or Keyence BZ-X810 microscope. The antibodies used for immunostaining can be
504 found in Supplementary Tables S4 and S5.

505

506 ***Flow cytometry***

507 Human iPSCs were harvested by incubation with EDTA for 3-5 mins followed by aspiration,
508 followed by gentle detachment with culture media. Cells were then transferred to 15 mL tubes
509 and centrifuged at 200 g for 5 mins. The supernatant was aspirated, and cells were resuspended
510 into single cells in filtered FACS buffer (PBS, 4% w/v bovine serum albumin (BSA), 10% v/v
511 Penicillin-Streptomycin (Pen-Strep), 4% v/v EDTA). After repeating the last step, the cells
512 were stained for 30 mins at RT. The antibodies used can be found in Supplementary Table S4-
513 5.

514

515 HiPSC-CMs were dissociated with the Cardiomyocyte Dissociation Kit (see above) and stained
516 with the Inside Stain Kit (Miltenyi Biotech) according to the manufacturer's protocol. Briefly,
517 dissociated cells are counted with Trypan Blue and up to 1 million cells are washed by adding
518 FACS buffer. After centrifugation at 200 g for 10 mins, the cells are resuspended in 1:1 FACS
519 buffer/Inside Fix buffer. After 20 mins of incubation in the dark at RT, the cells are washed
520 with FACS buffer and centrifuged at 200 g for 5 mins. The washing step is repeated in Inside
521 Perm. The cells were directly stained in Inside Perm buffer for 10-30 mins at RT, or indirectly
522 for 1h at RT and with secondary antibodies for 30 mins at RT in the dark. The antibodies used
523 can be found in Supplementary Table S4-5.

524 HiPSCs/hiPSC-CMs were subsequently washed and resuspended in incubation medium and
525 were kept on ice until analysis. Data was acquired on a BD LSRFortessa instrument and
526 analysed using FlowJo software.

527

528 ***Real-time quantitative PCR (RT-qPCR)***

529 Total RNA isolation was performed using the RNeasy mini kit (Qiagen) according to the
530 manufacturer’s protocol. Briefly, harvested cells or heart homogenates were lysed in RLT lysis
531 buffer for 5 mins at RT. The resulting cell lysate was transferred to a QIAShredder column and

532 was centrifuged at full speed for 3 mins. Next, 70% ethanol was added to the lysate, which was
533 transferred to an RNeasy silica column, followed by centrifugation at 1.2 x 10^4 rpm for 15s.
534 This was followed by a washing step in RW1 wash buffer and a DNase I incubation for 15 mins
535 at RT, followed by another wash step with RW1 and twice with RPE, followed by dry
536 centrifugation of the column at 1.2 x 10^4 rpm for 1 min. The RNA was eluted in RNase free
537 ddH2O for 2 min at RT followed by centrifugation at 1.2 x 10^4 rpm for 1 min. Eluted RNA was
538 kept on ice until further use or stored at -80°C for future use. RNA was subsequently reverse
539 transcribed into cDNA with the High Capacity Reverse Transcription Kit (Thermofisher,
540 4368814) with the following thermal cycler settings: 10 min at 25°C, 120 mins at 37°C, 5 mins
541 at 85°C. Gene expression was quantified by real-time PCR of 10 ng cDNA of each sample with
542 the PowerUp SYBR Green supermix (Thermofisher, A257420). Primers for each gene are
543 given in Table S6. β-actin and GAPDH were used as housekeeping genes. Of note, the use of
544 β-actin and GAPDH as reference genes has been critiqued as these genes show variable levels
545 of expression in different tissues during development including the heart, which might
546 compromise their role in gene expression normalisation (Lin & Redies, 2012).
547 The plate was transferred to a QuantStudio 7.0 Real-Time PCR machine (Applied Biosystems)
548 and the following parameters were applied: 5 mins 95°C, 40 cycles of 15s at 95°C, 30s at 60°C
549 and 30s at 72°C, followed by a melt curve analysis from 55-95°C.
550
551 ***Statistics***

552 All data was analysed using Graphpad Prism 9.0 software (Graphpad, San Diego, CA). Data is
553 represented as mean ± standard deviation (SD). Statistical analysis was performed on data with
554 a replicate number of 3 and above. Technical replicates are indicated with 'n' and biological
555 replication with 'N', as detailed in the figure legends. For the comparison between two groups,
556 two-tailed unpaired Student's t-tests were performed. Multiple group comparisons were

557 performed with one-way or two-way analysis of variance (ANOVA) with Tukey's post hoc test
558 correction (3 groups) or Dunnett's correction (>3 groups). If the number of replicates was not
559 equal between groups, a mixed-effects analysis was performed instead of an ANOVA, as the
560 latter cannot deal with missing values. Statistical significance was accepted at $p < 0.05$.

561

562 **AUTHOR CONTRIBUTIONS**

563 KS, FLM and LD conceived and designed the study. LD performed the majority of the
564 experiments. KK and AHAG contributed to the execution of select experiments. LD, KS and
565 FLM analysed the data and wrote the manuscript. All the authors read and approved the
566 manuscript.

567

568 **COMPETING INTERESTS STATEMENT**

569 The authors declare that they have no competing financial interests.

Figure 1

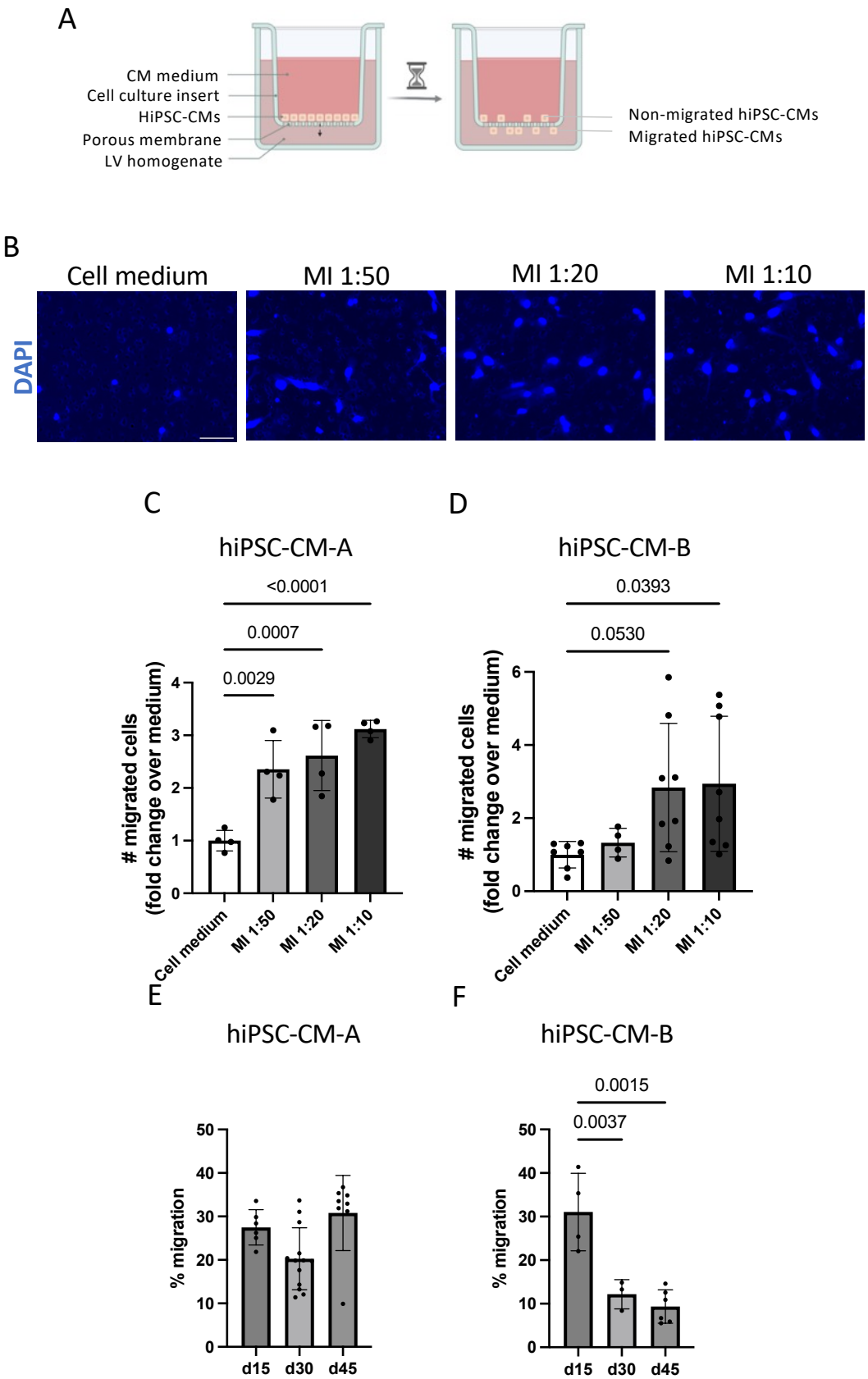

FIG 1. Human iPSC-CMs show a concentration-dependent chemotactic response to an MI stimulus that varies with maturation stage. A) Schematic of the transwell migration assay. B-D) HiPSC-CMs were seeded at day 15 and fixed and stained at 24h after incubation with cell medium, non-MI or MI homogenate at different dilutions. Non-migrated hiPSC-CMs on the top of the membrane were swabbed away and migrated hiPSC-CMs were imaged. B-C) hiPSC-CM-A, n=4. DAPI staining was used to visualise nuclei. Scale bar: 50 µm. D) hiPSC-CM-B, n=4-8, N=2. E-F) hiPSC-CM-A and hiPSC-CM-B were seeded at different days of differentiation and fixed and stained at 24h after incubation with MI homogenate (1:10), n= 6-10, N=1-3 (E), n=3-6, N=1-2 (F). Technical replicates are indicated with 'n' and biological replication with 'N'. Statistical analyses were performed using one-way ANOVA with Dunnett's correction. Error bars indicate mean ± SD.

Figure 2

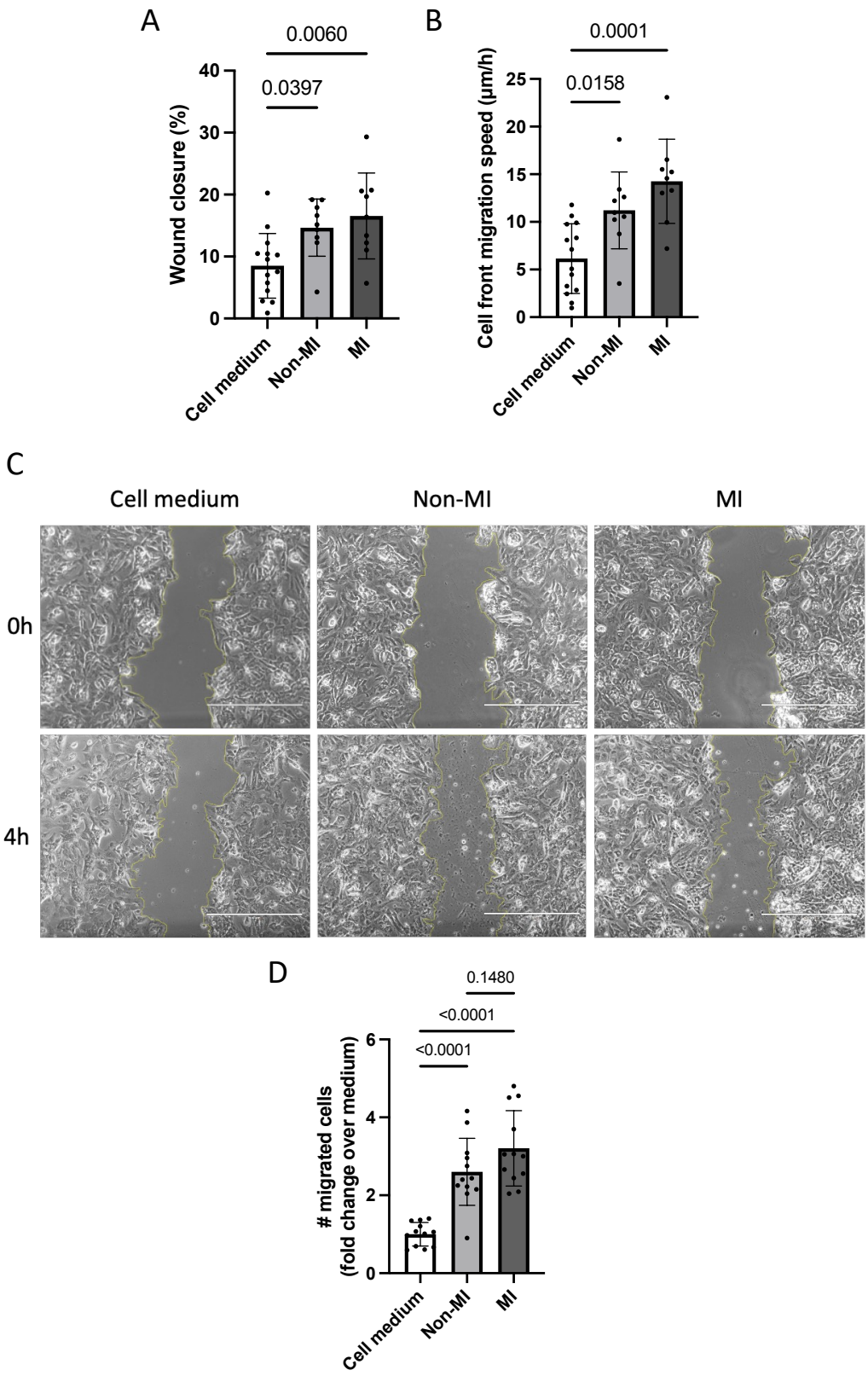

FIG 2. Human iPSC-CMs show a two-fold increase in migration when exposed to an MI environment. A-C) Day 15 hiPSC-CM-D (commercial kit) were replated to form a monolayer and a scratch was generated. HiPSC-CM-D were incubated with cell medium only (n=14) or supplemented with MI (1:10, n=9) or non-MI homogenate (1:10, n=9), wound closure (A) and cell front migration speed (B) were measured after 4h of incubation, N=2. C) Representative images of day 15 hiPSC-CM-D in the scratch wound assay. Scale bar: 1000 µm. D) Day 15 hiPSC-CM-A were seeded on transwell inserts and exposed to a 1:20 dilution of MI or non-MI homogenate for 4h (n=12). Technical replicates are indicated with 'n' and biological replication with 'N'. Statistical analyses were performed using a one-way ANOVA followed by Tukey's pairwise comparisons. Error bars indicate mean ± SD.

Figure 3

A

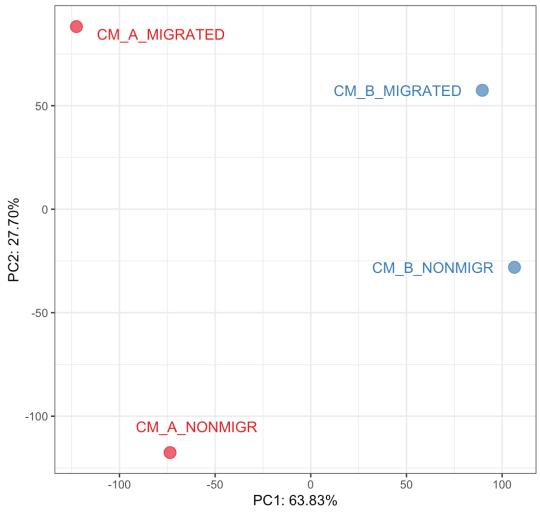

C

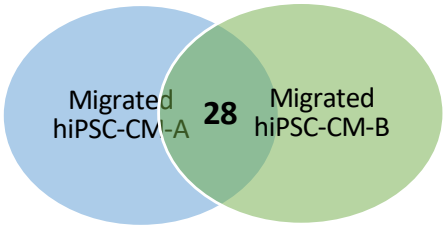

D

PTX3	SOX17	BMP6	TGFBI	SPP1
NTM	GLIPR1	VIPR1	RGPD6	NT5E
CASP4	OAS3	F2RL2	BGN	CLMP
EPAS1	NFE2L3	KCNJ2	KIF18B	MKI67
HMGA2	VEPH1	F2RL3	CDK1	SLC7A11
DACT2	NEK2	DHRS2		

B

hiPSC-CM-A

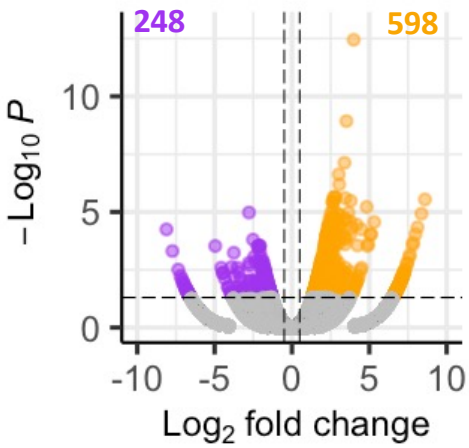

hiPSC-CM-B

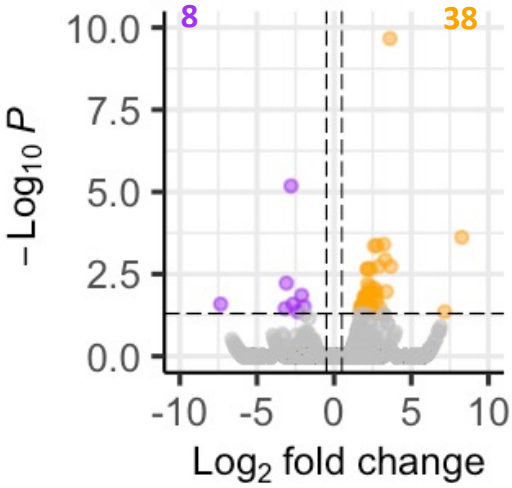

E

Cellular and molecular functions associated with hiPSC-CM migration	
hiPSC-CM-A	
Cellular and molecular function	P-value range
Cell Cycle	4.77E-11 – 1.64E-29
Cellular Assembly and Organization	4.60E-11 – 1.64E-29
DNA Replication, Recombination, and Repair	4.60E-11 – 1.64E-29
Cellular Movement	2.47E-11 – 2.69E-23
Cell Death and Survival	6.70E-12 – 8.52E-23
hiPSC-CM-B	
Cellular and molecular function	P-value range
Cellular Development	1.21E-03 – 3.45E-08
Cell Cycle	8.86E-04 – 8.79E-08
Cell Death and Survival	1.03E-03 – 3.17E-07
Cellular Movement	1.34E-03 – 3.53E-07
Cell Morphology	1.37E-03 – 6.22E-07

FIG 3. Migrated and non-migrated hiPSC-CMs represent distinct populations after 24h of incubation with MI homogenate. HiPSC-CM-A and hiPSC-CM-B were seeded on transwell inserts at day 15. After incubation overnight, the hiPSC-CMs were exposed to a 1:10 dilution of MI homogenate for 24h. Subsequently, migrated and non-migrated cells were harvested separately and analysed by bulk RNAseq. A) PCA plot. B) Differentially expressed genes in migrated cells versus non-migrated cells in hiPSC-CM-A and hiPSC-CM-B after 24h. Red dots indicate significantly upregulated genes, green dots indicate significantly downregulated genes and blue dots indicate genes which are not significantly differentially expressed. The cut-off parameters were chosen as log2FoldChange > |1| and padj or false discovery rate (FDR) <0.05. C-D) Combining the datasets resulted in a panel of 28 shared genes. E) Cellular and molecular functions associated with hiPSC-CM migration generated from the 24h dataset via Ingenuity Pathway Analysis.

Figure 4

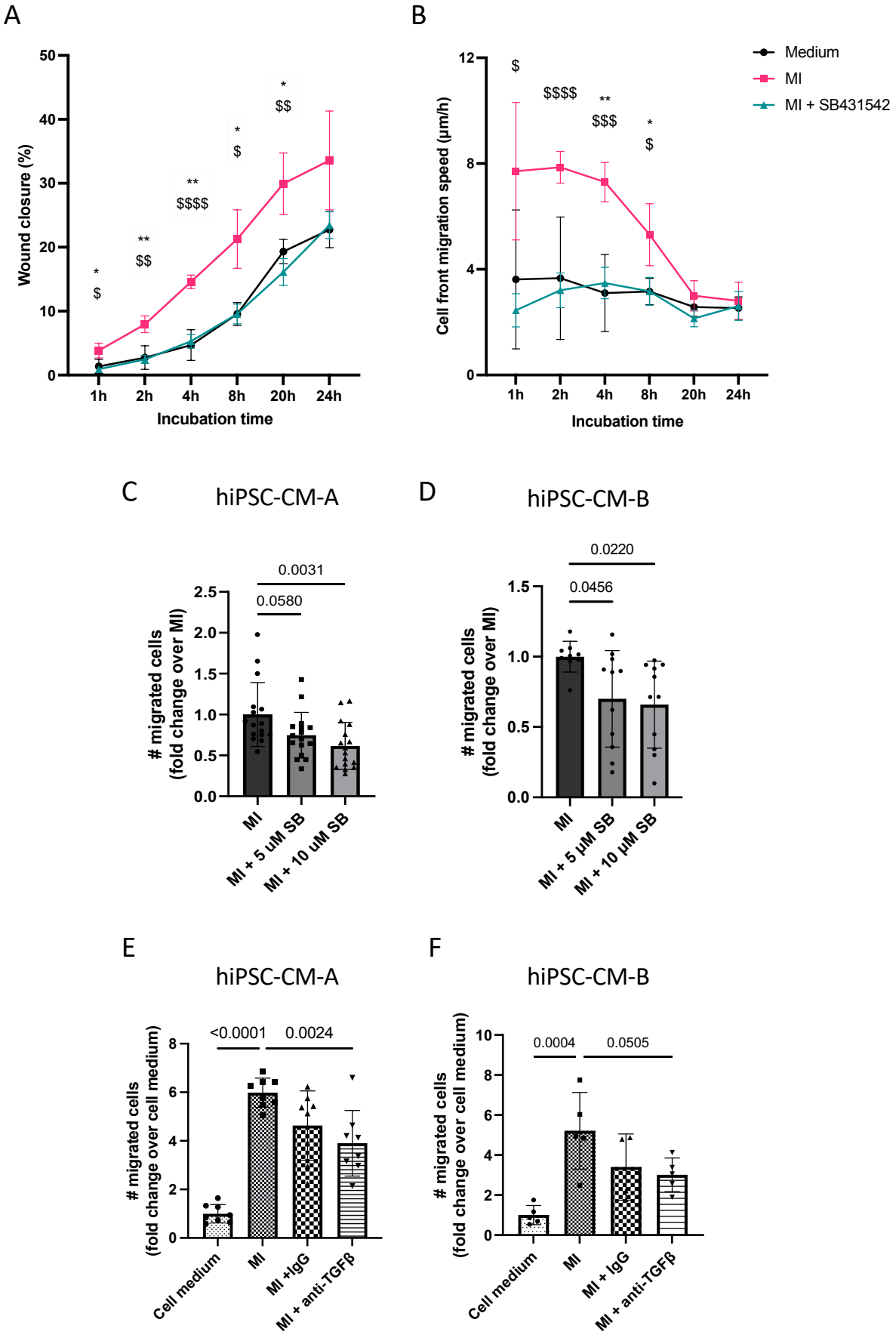

FIG 4. Inhibiting TGF-β signalling decreases MI-induced hiPSC-CM migration. A-B) Day 15 hiPSC-CM-A were seeded overnight and incubated with medium, MI 1:20 or MI 1:20 supplemented with 10 µM SB431542, n=4. *: P<0.05, **: P<0.01, MI vs. medium, $: P<0.05, $$: P<0.01, $$$: P<0.001, $$$$: P<0.0001, MI vs. MI + SB431542. C-D) HiPSC-CMs were seeded on transwell inserts and exposed to MI 1:20 only or with a 15-minute pre-incubation of 5 µM or 10 µM SB431542 prior to incubation with MI for 4h. C) hiPSC-CM-A, N=2 (d15 and d16), n=16. D) hiPSC-CM-B, N=3 (d15), n=10-11. E-F) D15 hiPSC-CMs were seeded on transwell inserts and exposed to cell medium, MI 1:20 only or MI with 20 ng/mL IgG or TGF-β neutralisation antibody for 4h. E) hiPSC-CM-A, n=12. F) hiPSC-CM-B, n=4-5. Technical replicates are indicated with 'n' and biological replication with 'N'. Statistical analyses were performed using a one-way ANOVA followed by Tukey's pairwise comparisons (C) or Dunnett's correction (D-F). Error bars indicate mean ± SD.

Figure S1

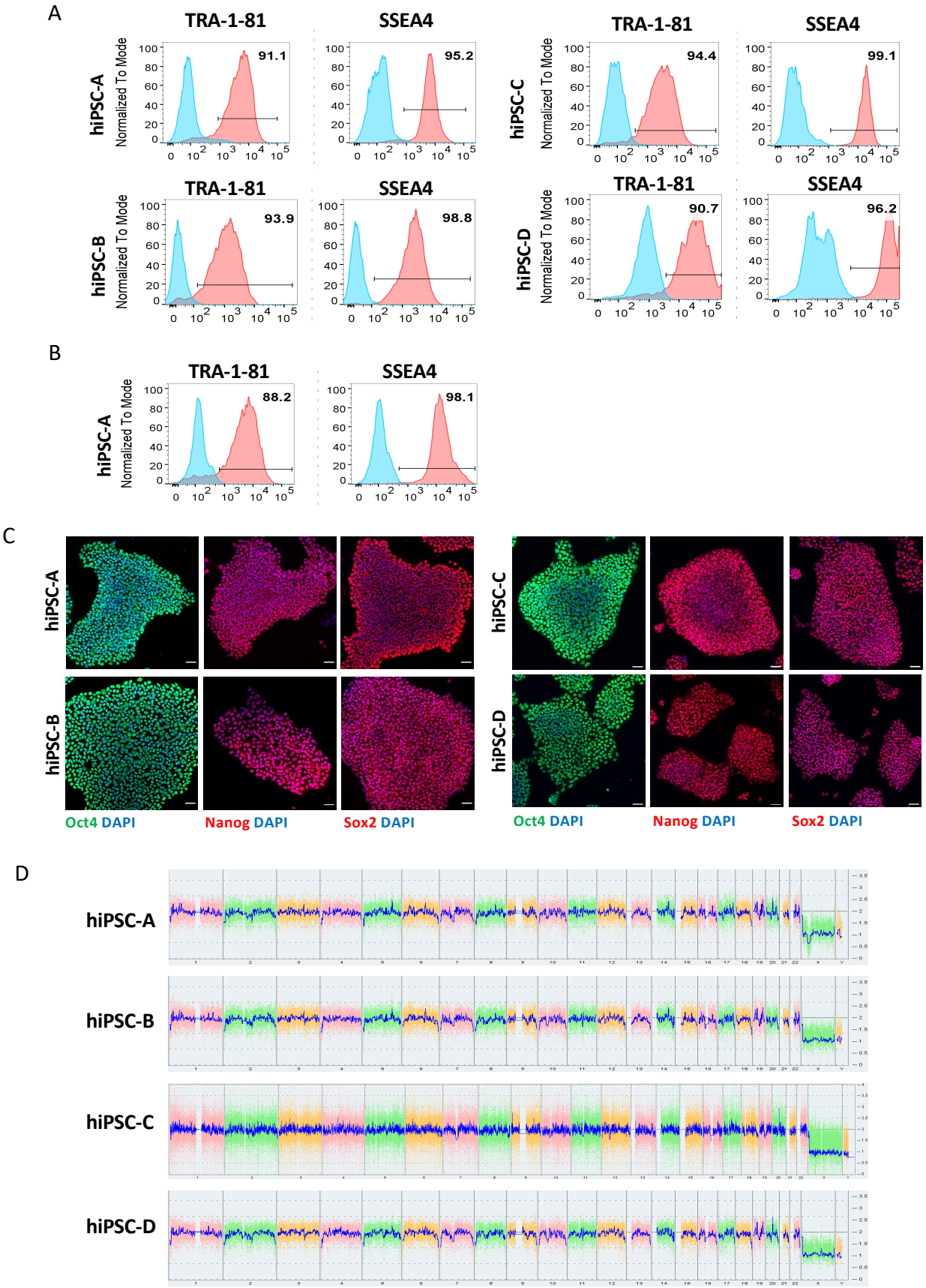

FIG S1: Pluripotency and karyotype normality of hiPSC lines. A) Flow cytometric analysis of pluripotency markers, TRA-1-81 and SSEA4 of hiPSC-A (P47), hiPSC-B (P34), hiPSC-C (P34) and hiPSC-D (P41). Samples are shown in red and isotype controls are shown in blue. B) Flow cytometric analysis of TRA-1-81 and SSEA4 of hiPSC-A at passage 77. C) Representative micrographs showing immunolabelling of pluripotency markers Oct-4 (green), Nanog (red) and Sox2 (red), nuclei are labelled with DAPI (blue). Scalebar: 50 µm. D) hiPSCs A-D were negative for karyotypic abnormalities confirmed by KaryoStat analysis at passage 54, 47, 36 and 44, respectively. The whole genome view displays all somatic and sex chromosomes in one frame with copy number levels. The pink, green and yellow colours indicate the raw signal for each individual chromosome probe, while the blue signal represents the normalized probe signal which is used to identify copy number and potential aberrations deviating from a normal copy number state (CN = 2).

Figure S2

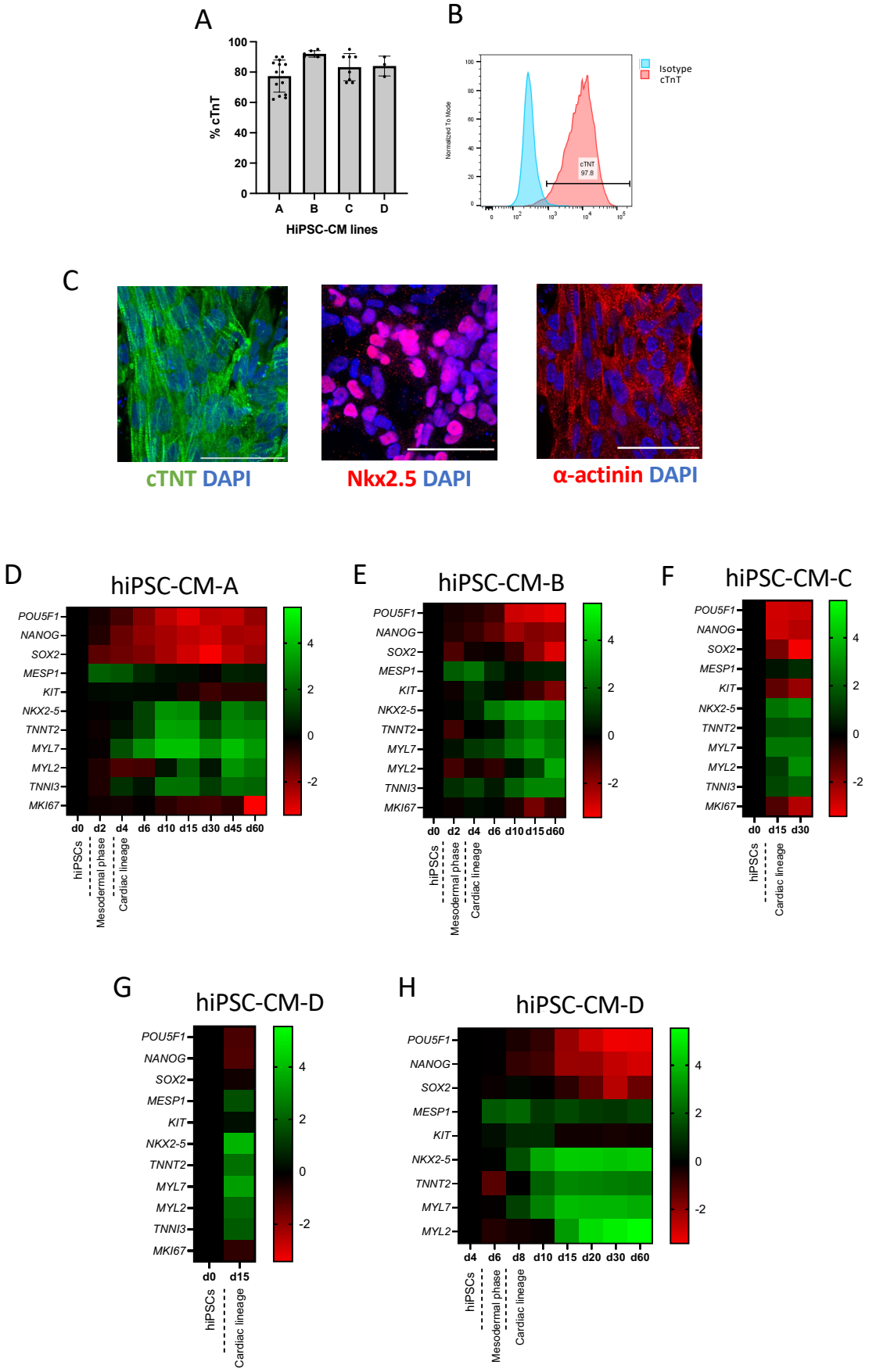

FIG S2: Expression of pluripotency and cardiac markers during hiPSC-CM differentiation using the Burridge protocol and commercial kit. A) Differentiation efficiency measured by cTnT expression in hiPSC-CM-A-D lines using the Burridge et al. protocol. B) Representative graph of cTnT expression measured in hiPSC-CM-B at day 15. C) Representative micrographs showing immunolabelling for cardiac markers at day 15 of hiPSC-CM-D differentiation using the commercial kit. Scalebar: 50 µm. D-H). Heat maps illustrating quantitative RT-qPCR analysis of pluripotent, mesodermal, and cardiac marker expression during hiPSC-CM differentiation of hiPSC-CM-A (D), hiPSC-CM-B (E), hiPSC-CM-C (F) and hiPSC-CM-D (G) using the Burridge protocol and hiPSC-CM-D using the commercial kit (H). Values are represented as log fold change and represent the average of 1-3 samples.

Figure S3

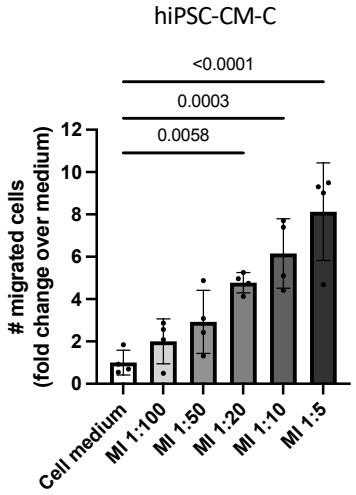

Fig S3: MI homogenate has a concentration-dependent effect on hiPSC-CM-C migration. HiPSC-CM-C were seeded onto transwells at day 15 and fixed and stained at 24h after incubation with cell medium, non-MI or MI homogenate at different dilutions. Non-migrated hiPSC-CMs on the top of the membrane were swabbed away and migrated hiPSC-CMs were imaged. n=4. Statistical analysis was performed using one-way ANOVA followed by Dunnett's correction. Error bars indicate mean $\pm$ SD.

Figure S4

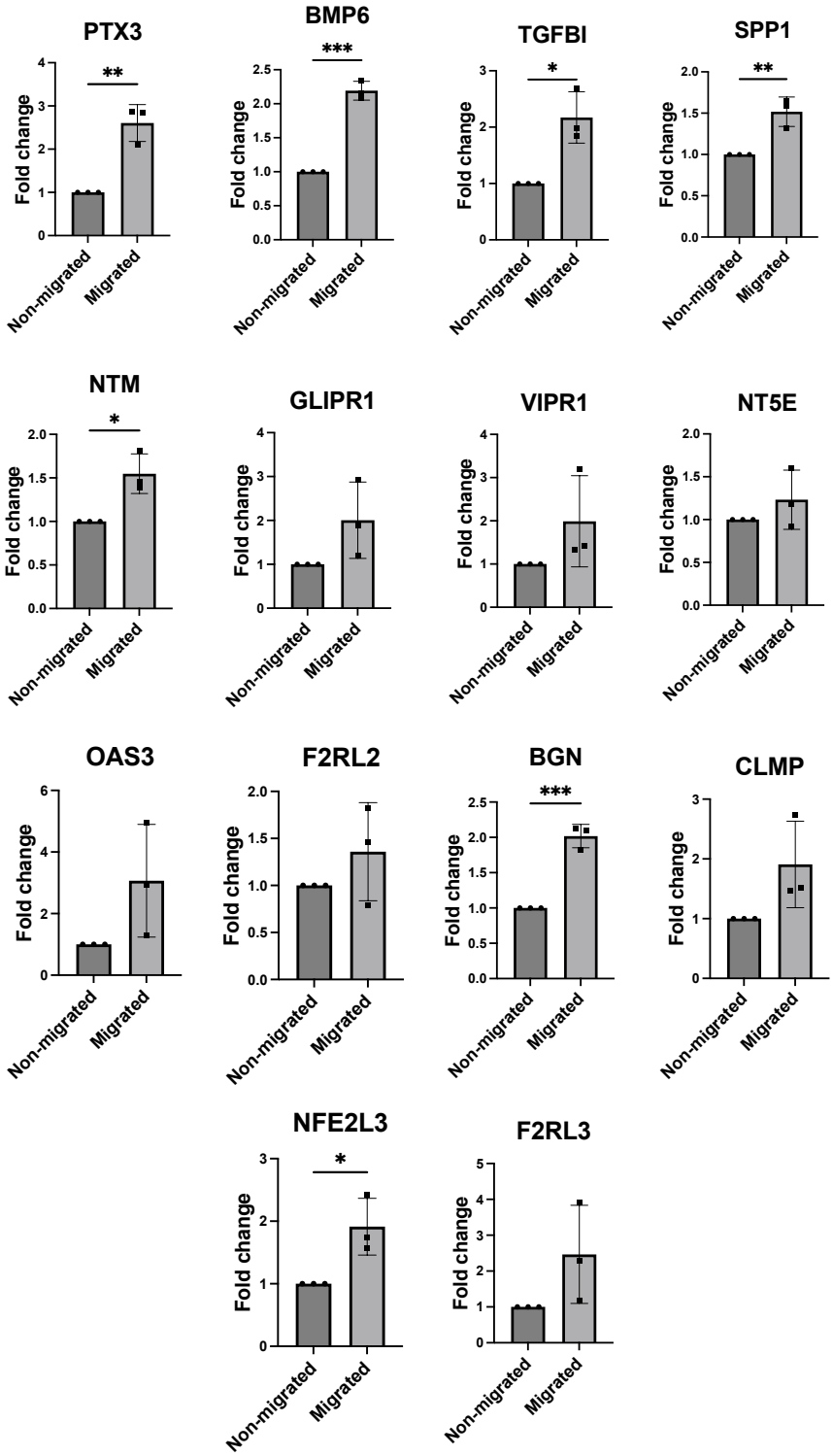

FIG S4: Differentially expressed gene verification comparing migrated hiPSC-CMs to their non-migrated counterparts. HiPSC-CM-A,-B and -C were seeded at day 15 on transwell inserts and exposed to MI 1:10 for 24h after which the non-migrated and migrated cells were harvested separately. RT-qPCR confirmed the upregulation of all 14 genes of interest in migrated cells compared to their non-migrated counterparts in all three biological replicates. Statistical analyses were performed using two-tailed, unpaired t-tests. Error bars indicate mean ± SD. *: $P \leq 0.05$, **: $P \leq 0.01$, ***: $P \leq 0.001$.

Figure S5

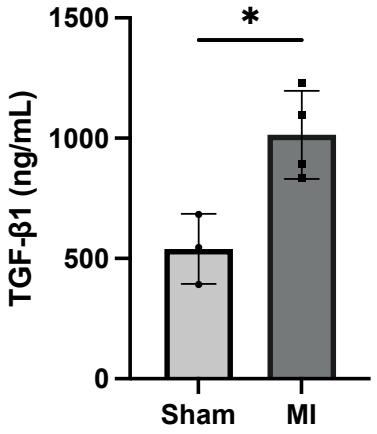

FIG S5: TGF-β1 levels in sham and MI rat left ventricular homogenates. TGF-β1 was measured in sham (n=3) or MI (n=4) LV homogenate samples by ELISA. Statistical analysis was performed using a two-tailed unpaired t-test. *, $P < 0.05$.

Table S1: Gene expression profiles of hiPSC-CMs analysed for bulk RNAseq after 24h of incubation with MI homogenate (1:10). Values represent normalised read counts. Padj = adjusted p-value or false discovery rate (FDR).

Gene	hiPSC-CM-A			hiPSC-CM-B		
	Migrated	Non-migrated	padj	Migrated	Non-migrated	padj
TNNT2	8071	18864	0.07	11685	16025	1
NKX2-5	3044	4933	0.48	3892	4316	1
MYL7	18495	44382	0.06	26798	38134	1
NR2F2	1109	487	0.10	746	540	1
MYL2	60	142	0.14	91	123	1
IRX4	126	254	0.23	291	257	1
TBX18	1193	779	0.56	206	85	0.59
HCN4	1458	2882	0.21	1097	1643	1
TNNI3	231	687	0.01	280	515	1
TNNI1	2620	6508	0.05	3499	5198	1
MYH6	26392	88865	0.003	14032	32149	0.53
MYH7	4489	16524	0.001	2285	4259	1
DDR2	806	403	0.21	599	284	0.84
THY1	368	149	0.07	30	5	0.23
CD31	-	-		-	-	

Table S2: Gene Ontology (GO) analysis of migrated versus non-migrated hiPSC-CM-Bs and hiPSC-CM-Cs after 24h of incubation with MI homogenate.

GOID	Description	GeneRatio	pvalue	padj
hiPSC-CM-A				
GO:0030198	extracellular matrix organization	86/1624	2.29E-15	1.20E-12
GO:0006935	chemotaxis	100/1624	2.08E-09	2.54E-07
GO:0042330	taxis	100/1624	2.34E-09	2.79E-07
GO:2000147	positive regulation of cell motility	90/1624	2.95E-09	3.45E-07
GO:0040017	positive regulation of locomotion	94/1624	3.75E-09	4.19E-07
GO:0031032	actomyosin structure organization	48/1624	8.57E-09	9.18E-07
GO:0030335	positive regulation of cell migration	86/1624	1.88E-08	1.90E-06
GO:0030048	actin filament-based movement	37/1624	1.93E-08	1.91E-06
GO:0060326	cell chemotaxis	41/1624	5.87E-05	0.002
GO:0050920	regulation of chemotaxis	36/1624	7.37E-05	0.002
GO:0050921	positive regulation of chemotaxis	25/1624	0.0003	0.005
GO:0006929	substrate-dependent cell migration	9/1624	0.001	0.01
GO:0042246	tissue regeneration	13/1624	0.001	0.01
GO:0014812	muscle cell migration	17/1624	0.005	0.04
hiPSC-CM-B				
GO:0006935	chemotaxis	25/421	0.0048	0.12
GO:0042330	taxis	25/421	0.0049	0.12
GO:2000147	positive regulation of cell motility	21/421	0.012	0.20
GO:0050921	positive regulation of chemotaxis	8/421	0.013	0.20
GO:0030335	positive regulation of cell migration	20/421	0.017	0.23
GO:0040017	positive regulation of locomotion	21/421	0.024	0.28
GO:0060326	cell chemotaxis	11/421	0.028	0.31

Table S3: Differentially expressed genes (DEGs) shared between migrated (A-M,B-M) versus non-migrated hiPSC-CM-A (A-NONM) and hiPSC-CM-B (B-NONM) after 24h of incubation with MI homogenate diluted 1:10. Values represent as normalised read counts. Padj = adjusted p-value or false discovery rate (FDR).

DEG	A-M	A-NONM	log2FC	padj A	B-M	B-NONM	log2FC	padj B
PTX3	4959.38	312.57	3.99	3E-13	1931.98	157.41	3.62	2E-10
SOX17	955.81	83.22	3.52	1E-09	160.50	23.36	2.77	0.0004
BMP6	1081.94	132.95	3.02	2E-07	161.49	32.50	2.31	0.008
TGFBI	9837.96	1522.27	2.69	2E-06	1024.09	229.51	2.16	0.002
SPP1	3503.99	565.27	2.63	3E-06	95.51	10.16	3.22	0.0004
NTM	936.10	133.96	2.80	2E-06	279.65	61.95	2.17	0.006
GLIPR1	1134.16	175.57	2.69	3E-06	192.02	49.76	1.95	0.034
VIPR1	144.85	13.19	3.44	2E-06	67.94	10.16	2.73	0.011
RGPD6	46.31	318.66	-2.78	1E-05	50.22	193.97	-1.95	0.031
NT5E	126.13	27.40	2.20	0.002	240.27	46.72	2.36	0.002
CASP4	217.77	48.71	2.16	0.001	81.73	13.20	2.62	0.009
OAS3	34.49	5.08	2.73	0.012	38.40	0.00	8.27	0.0002
F2RL2	434.55	113.66	1.93	0.002	151.64	31.48	2.26	0.011
BGN	319.26	77.13	2.05	0.001	93.55	17.27	2.43	0.012
CLMP	773.52	259.80	1.57	0.014	509.09	134.05	1.92	0.016
EPAS1	1503.68	459.73	1.71	0.005	208.76	49.76	2.07	0.016
NFE2L3	205.94	37.55	2.45	0.0002	222.54	53.82	2.05	0.016
KCNJ2	76.86	8.12	3.22	9E-05	55.14	8.13	2.74	0.020
KIF18B	692.72	157.30	2.14	0.0003	331.84	88.35	1.91	0.024
MKI67	1768.74	360.27	2.30	6E-05	986.67	286.38	1.78	0.029
HMGA2	11854.04	3122.68	1.92	0.001	5456.22	1629.94	1.74	0.029
VEPH1	59.12	15.22	1.95	0.029	97.48	21.33	2.19	0.029
F2RL3	79.81	23.34	1.77	0.030	100.44	22.34	2.16	0.030
CDK1	1067.16	276.04	1.95	0.001	606.57	176.70	1.78	0.034
SLC7A11	10478.46	3401.76	1.62	0.008	11840.03	3683.36	1.68	0.039
DACT2	102.48	21.31	2.26	0.002	17.72	0.00	7.16	0.044
NEK2	332.07	87.28	1.93	0.003	156.57	40.62	1.94	0.045
DHRS2	19.71	2.03	3.20	0.035	45.29	194.98	-2.10	0.014

Table S4. List of unconjugated antibodies used in this study. All antibodies are reactive against human. ICC: immunohistochemistry, WB: western blot, FC: flow cytometry.

Target	Host species	Source	Application	Working concentration
Oct3/4	Goat	R&D, #AF1759	ICC	1:50
Nanog	Goat	R&D, #AF1997	ICC	1:50
Sox2	Rabbit	Abcam, #Ab97959	ICC	1:500
Nkx2.5	Goat	R&D, #AF2444	ICC	1:20
cTNT	Mouse	Thermofisher, #MA5-12960	ICC, WB, FC	1:50
Sarcomeric alpha-actinin	Mouse	Sigma (Merck), #A7811	ICC	1:250
MLC2v	Rabbit	Proteintech, #10906-1-AP	FC	1:400

Table S5. List of conjugated antibodies used in this study. ICC: immuno-histochemistry, WB: western blot, FC: flow cytometry.

Target	Conjugate	Source	Application	Working concentration
Anti-mouse	AF488	Thermofisher, #A21202	ICC	1:500
Anti-mouse	AF647	Thermofisher, #A21242	FC	1:500
Anti-goat	AF488	Thermofisher, #A11055	ICC	1:500
Anti-goat	AF594	Thermofisher, #A11058	ICC	1:500
Anti-rabbit	AF488	Thermofisher, #A21206	ICC	1:500
Anti-rabbit	AF555	Thermofisher, #A32732	FC	1:500
Anti-rabbit	AF594	Thermofisher, #A11037	ICC	1:500
Anti-human TRA-1-81 (IgM, κ)	AF488	Biolegend, #330710	FC	1:10
Anti-human isotype (IgM, κ)	AF488	Biolegend, #401617	FC	1:10
Anti-human SSEA4 (IgG3)	AF488	Thermofisher, #53-8843-42	FC	1:10
Anti-human isotype (IgG3)	AF488	Biolegend, #401324	FC	1:10
Anti-human cTnT (IgG1)	FITC	Miltenyi, #130-119-575	FC	1:50
Anti-human isotype control (IgG1)	FITC	Miltenyi, #130-118-354	FC	1:50

Table S6: Forward and reverse primer sequences for the genes of interest for RT-qPCR. All primers have a melting temperature of approximately 60°C.

Gene	Primer sequence	
	Forward (5'-3')	**Reverse (5'-3')**
POU5F1	CAAAGCAGAAACCCTCGTGC	CTCGGACCACATCCTTCTCG
SOX2	GGGGAAAGTAGTTTGCTGCC	CGCCGCCGATGATTGTTATT
NANOG	CTGCAGAGAAGAGTGTCGCA	ACCAGGTCTTCACCTGTTTGT
MESP1	ACGGTCCCCGCTCCTTC	CAGTCTGCCAAGGAACCACT
KIT	AGGAAACGCTCGACTACCTG	CATTCCAGGATAGGGGCTGC
NKX2-5	CAAGTGTGCGTCTGCCTTTC	CGCACAGCTCTTTCTTTTCGG
TNNT2	ATCCTCTGCCTCACCCAGTC	GCTCTCCCTCAGAACAGCAG
MYL2	CAATTAACTTTACTGTGTTCCTCACAA	GAACGTAATCAGCCTTCAGCAC
MYL7	CCGTCTTCCTCACGCTCTT	TGAACTCATCCTTGTTCACCAC
PTX3	CGTCTCTCCAGCAATGCATC	AAGAGCTTGTCCCATTCCGA
BMP6	CCGACAACAGAGTCGTAATCGC	CTGCCATCCCAGGTCTTGGAAA
TGFBI	ATGACCCTCACCTCTATGTACC	CACAGTTCACAGTTACAATCCCA
SPP1	GCCGAGGTGATAGTGTGGTT	AACGGGGATGGCCTTGTATG
NTM	TGCTGTTCCTTGTACCCACAGG	CGAGGATCCAGGCACCACT
GLIPR1	GGCTTTGACGCTCTTTCCAA	CGTTTGACTTGGTCTCGCTGT
VIPR1	GGACACCATCAACTCCTCACTG	CGCAGTTTCTGAAGCAGGATTCG
NT5E	TCTTCTAAACAGCAGCATTCC	CATTTCATCCGTGTGTCTCAG
OAS3	CCTGATTCTGCTGGTGAAGCAC	TCCCAGGCAAAGATGGTGAGGA
F2RL2	TCCTGGTGTTTGTAGTTGGTGT	CCAGTTGTTCCCATTGAGATGA
BGN	TGACTGGCATCCCCAAAGAC	GAGTAGCGAAGCAGGTCCTC
CLMP	TTACTGGCAGCGAATCCGAGAG	CTGGTACAGTCCAGAGTAGGAC
NFE2L3	CCAGTTGCTTTCATCACAGCCTG	CACATCCTGACTTATAGCCTGGC
F2RL3	ACCGGAGGTGGTGATGACAG	CACAGACTTGGCCTGGGTAG
GAPDH	GTCAAGGCTGAGAACGGGAA	AAATGAGCCCCAGCCTTCTC
ACTB	GTGGCATCCACGAAACTACC	GTACTTGCGCTCAGGAGGAG